

On the Shapes of Interstellar Grains: Modeling Infrared Extinction and Polarization by Spheroids and Continuous Distributions of Ellipsoids

B. T. DRAINE¹ AND BRANDON S. HENSLEY^{1,2}

¹*Department of Astrophysical Sciences, Princeton University, Princeton, NJ 08544-1001, USA*

²*Spitzer Fellow*

ABSTRACT

Although interstellar grains are known to be aspherical, their actual shapes remain poorly constrained. We assess whether three continuous distributions of ellipsoids (CDEs) from the literature are suitable for describing the shapes of interstellar grains. Randomly-selected shapes from each distribution are shown as illustrations. The often-used Bohren-Huffman CDE includes a very large fraction of extreme shapes: fully 10% of random draws have axial ratio $a_3/a_1 > 19.7$, and 5% have $a_3/a_1 > 33$. The CDE2 distribution includes a much smaller fraction of extreme shapes, and appears to be the most realistic. For each of the three CDEs considered, we derive shape-averaged cross sections for extinction and polarization in the Rayleigh limit. Finally, we describe a method for “synthesizing” a dielectric function for an assumed shape or shape distribution if the actual absorption cross sections per grain volume in the Rayleigh limit are known from observations. This synthetic dielectric function predicts the wavelength dependence of polarization, which can then be compared to observations to constrain the grain shape.

Keywords: dust, extinction

1. INTRODUCTION

After many years of study, both the composition and the geometry (shape, porosity) of interstellar grains remain uncertain. While meteorites can provide samples of presolar grains that were part of the interstellar grain population at the time of formation of the solar system, the surviving particles may not be representative, and the sampling techniques are biased toward large “stardust” grains with isotopic anomalies. Interstellar grains collide with interplanetary spacecraft, providing some information on elemental composition, but the data are limited and generally involve vaporization of the impinging particle, leaving both mineralogy and preimpact morphology uncertain (e.g., [Altobelli et al. 2016](#)). The Stardust mission captured some particles relatively intact ([Westphal et al. 2014a,b](#)), but dynamical considerations argue against these particles having come from the interstellar medium ([Silsbee & Draine 2016](#)).

As a result, our knowledge of interstellar grains is based almost entirely on (1) evidence of elements that have been “depleted” from interstellar gas and incorporated into dust grains, and (2) observations of the interaction of electromagnetic waves with the interstellar grains – absorption, scattering, and emission ([Hensley & Draine 2021](#)). The challenge to grain modelers is to create physical models that are consistent with these constraints.

Corresponding author: B. T. Draine

draine@astro.princeton.edu, bhensley@astro.princeton.edu

©2020. All rights reserved.

Grain models must specify the optical properties of the grain materials, and the shapes and sizes of the grains. The optical properties of a grain, particularly for polarization, depend on the grain shape, i.e., morphology. Because the universe of possible grain morphologies is unbounded, modelers are forced to limit consideration to some subset of idealized shapes. With stringent constraints now available for polarized extinction by and emission from interstellar grains, the assumption of spherical grains is no longer adequate for modeling. The natural first step beyond spheres is to consider spheroids and ellipsoids.

The present work has two aims. The first is to discuss certain distributions of ellipsoidal shapes. Continuous distributions of spheroidal or ellipsoidal shapes have been considered in some previous studies, but the discussions have generally been limited to the angle-averaged absorption cross sections, with little said about the actual distribution of *shapes*. Here we explicitly discuss the distribution of shapes associated with three particular continuous distributions of ellipsoids (CDEs). We also derive the polarization cross sections for the CDEs for grains in the “electric dipole” or Rayleigh limit when the grains are not randomly oriented.

The second aim is to present a method for using observational constraints on absorption at long wavelengths, plus a prior estimate of the dielectric function at shorter wavelengths, to derive the complex dielectric function $\epsilon(\lambda)$ at long wavelengths λ . Absorption and polarization by grains both depend on the grain shape, or distribution of shapes. If we knew the dielectric function $\epsilon(\lambda)$, we could (at least in principle) infer the actual grain shape by computing absorption vs. λ for different assumed shape distributions, and seeing which shape distribution best agrees with observations. Because the actual grain materials remain unknown, we don’t know $\epsilon(\lambda)$, and hence cannot use that approach to deduce the grain shape. However, if we have observations of both absorption *and* polarization, we can determine which shape distribution yields a dielectric function that is consistent with both. We show here how this can be done. The methods developed here have been employed to obtain a dielectric function for “astrodust” (Draine & Hensley 2021) for continuous distributions of ellipsoids.

The paper is organized as follows: absorption and polarization cross sections for ellipsoids in the long wavelength (Rayleigh) limit are reviewed in section 2. In section 3 we discuss the properties of three continuous distributions of ellipsoidal shapes – the BHCDE, ERCDE, and CDE2 distributions – and present images of shapes drawn randomly from each of these distributions. Analytic results for polarized absorption cross sections are presented in sections 4 and 5. Attenuation and polarization by a medium with partial grain alignment is discussed in section 6. In section 7 we develop a method for employing the results obtained here, together with other constraints, to obtain a self-consistent dielectric function given observations of absorption as a function of wavelength. Our results are summarized in section 9. Certain technical results are collected in Appendices A–D.

2. ABSORPTION IN THE RAYLEIGH LIMIT

In the Rayleigh limit (grain size \ll wavelength λ), the interaction of a grain with an incident electromagnetic wave is fully characterized by the grain’s electric polarizability tensor (see, e.g., Draine & Lee 1984). Here we review the dependence of this polarizability tensor on the grain shape.

2.1. Ellipsoidal Grains

Consider an ellipsoidal grain with semimajor axes $a_1 \leq a_2 \leq a_3$ and volume $V = (4\pi/3)a_1a_2a_3$. Let $\hat{\mathbf{a}}_1, \hat{\mathbf{a}}_2, \hat{\mathbf{a}}_3$ be unit vectors along the three principal axes. We define an effective radius $a_{\text{eff}} \equiv (3V/4\pi)^{1/3} = (a_1a_2a_3)^{1/3}$.

The grain material is assumed to have an isotropic complex dielectric function $\epsilon(\lambda) = \epsilon_1 + i\epsilon_2$, where $\epsilon_1(\lambda)$ and $\epsilon_2(\lambda)$ are the real and imaginary parts of ϵ , and λ is the wavelength *in vacuo*. In the long-wavelength limit $a_3 \ll \lambda$, the electric polarizability tensor for radiation with $\mathbf{E} \parallel \hat{\mathbf{a}}_j$ is $\alpha_{jj} = A_j V/4\pi$, where

$$A_j(\epsilon) = \frac{\epsilon - 1}{1 + L_j(\epsilon - 1)}, \quad (1)$$

with L_j given by (see, e.g., [Bohren & Huffman 1983](#))

$$L_j = \frac{1}{2} \int_0^\infty \frac{dx}{[y_j^2 + x] [(y_1^2 + x)(y_2^2 + x)(y_3^2 + x)]^{1/2}} \quad (2)$$

$$y_j \equiv \frac{a_j}{(a_1 a_2 a_3)^{1/3}} \quad . \quad (3)$$

The L_j , referred to variously as “geometrical factors,” “shape factors,” or “depolarization factors,” are determined by the axial ratios a_1/a_3 and a_2/a_3 . The L_j satisfy

$$L_1 + L_2 + L_3 = 1 \quad . \quad (4)$$

If $a_1 \leq a_2 \leq a_3$, then

$$L_1 \geq L_2 \geq L_3 \quad . \quad (5)$$

The absorption cross section for radiation with $\mathbf{E} \parallel \hat{\mathbf{a}}_j$ is

$$C_{\text{abs},j} = \frac{2\pi V}{\lambda} \text{Im}(A_j) \quad . \quad (6)$$

After propagating a distance z through a medium with dust number density n_d , a plane wave will undergo both attenuation (due to absorption) and a phase shift relative to propagation *in vacuo*. The phase shift (in radians) will be $n_d C_{\text{pha}} z$, where

$$C_{\text{pha},j} = \frac{\pi V}{\lambda} \text{Re}(A_j) \quad . \quad (7)$$

The axes $\hat{\mathbf{a}}_1, \hat{\mathbf{a}}_2, \hat{\mathbf{a}}_3$ coincide with the principal axes of the moment of inertia tensor, with eigenvalues $I_1 \geq I_2 \geq I_3$. For randomly-oriented grains the absorption cross section is

$$C_{\text{ran}} = \frac{C_{\parallel} + 2C_{\perp}}{3} = \frac{2\pi V}{\lambda} \text{Im} \left(\frac{A_1 + A_2 + A_3}{3} \right) \quad . \quad (8)$$

Interstellar grains are generally spinning rapidly, and it is appropriate to average over the grain orientations. The direction of the grain axis $\hat{\mathbf{a}}_1$ may be correlated with the angular momentum vector \mathbf{J} ; if the grains are in suprathermal rotation, $\hat{\mathbf{a}}_1$ will tend to be aligned with \mathbf{J} , as originally pointed out by [Purcell \(1979\)](#). The absorption cross sections for $\mathbf{E} \parallel \hat{\mathbf{a}}_1$ and $\mathbf{E} \perp \hat{\mathbf{a}}_1$ are

$$C_{\parallel} \equiv C_{\text{abs}}(\mathbf{E} \parallel \hat{\mathbf{a}}_1) = \frac{2\pi V}{\lambda} \text{Im}(A_1) \quad (9)$$

$$C_{\perp} \equiv C_{\text{abs}}(\mathbf{E} \perp \hat{\mathbf{a}}_1) = \frac{2\pi V}{\lambda} \text{Im} \left(\frac{A_2 + A_3}{2} \right) \quad , \quad (10)$$

where the grains are assumed to be spinning with $\hat{\mathbf{a}}_2$ and $\hat{\mathbf{a}}_3$ randomly-distributed in the plane \perp to $\hat{\mathbf{a}}_1$.

Consider the limiting case of spinning grains that are perfectly-aligned with $\hat{\mathbf{a}}_1 \parallel \mathbf{J}$. For unpolarized radiation propagating with wavevector $\mathbf{k} \perp \mathbf{J}$, the polarization-averaged absorption cross section is

$$C_{\text{abs}} = \frac{C_{\perp} + C_{\parallel}}{2} = \frac{2\pi V}{\lambda} \text{Im} \left(\frac{A_2 + A_3 + 2A_1}{4} \right) \quad . \quad (11)$$

The difference in absorption cross sections will produce linear polarization, characterized by the “polarization cross section”

$$C_{\text{pol}} = \frac{C_{\perp} - C_{\parallel}}{2} = \frac{2\pi V}{\lambda} \text{Im} \left(\frac{A_2 + A_3 - 2A_1}{4} \right) \quad . \quad (12)$$

There will also be a phase shift between the two linear polarizations. We define

$$\Delta C_{\text{pha}} \equiv C_{\text{pha},\perp} - C_{\text{pha},\parallel} = \frac{\pi V}{\lambda} \text{Re} \left(\frac{A_2 + A_3 - 2A_1}{2} \right) . \quad (13)$$

After propagating a distance z through a medium with dust number density n_d , the phase difference between the modes will be $n_d \Delta C_{\text{pha}} z$. If the direction of grain alignment rotates along the direction of propagation, radiation that is initially unpolarized will develop circular polarization (Martin 1972, 1974). We define a “circular polarization efficiency factor”

$$Q_{\text{cpol}} \equiv \frac{C_{\text{pol}}}{\pi a_{\text{eff}}^2} \times \frac{\Delta C_{\text{pha}}}{\pi a_{\text{eff}}^2} . \quad (14)$$

If the rotation angle is small, and the percentage linear polarization is small, the circular polarization after propagating a pathlength z has Stokes parameters V and I varying as

$$\frac{V}{I} \propto Q_{\text{cpol}} \times (n_d \pi a_{\text{eff}}^2 z)^2 . \quad (15)$$

2.2. Spheroids

Prolate spheroids have $a_1 = a_2 < a_3$, and oblate spheroids have $a_1 < a_2 = a_3$. The “shape factors” L_j are given by (van de Hulst 1957)

$$\text{prolate : } L_3 = \frac{1 - e^2}{e^2} \left[\frac{1}{2e} \ln \left(\frac{1 + e}{1 - e} \right) - 1 \right] < 1/3 , \quad e^2 \equiv 1 - \left(\frac{a_1}{a_3} \right)^2 \quad (16)$$

$$L_1 = L_2 = \frac{1 - L_3}{2} \quad (17)$$

$$\text{oblate : } L_1 = \frac{1 + e^2}{e^2} \left[1 - \frac{1}{e} \arctan(e) \right] > 1/3 , \quad e^2 \equiv \left(\frac{a_3}{a_1} \right)^2 - 1 \quad (18)$$

$$L_2 = L_3 = \frac{1 - L_1}{2} . \quad (19)$$

A sphere has $(L_1, L_2, L_3) = (\frac{1}{3}, \frac{1}{3}, \frac{1}{3})$; the prolate limit (needle-like) has $(L_1, L_2, L_3) = (\frac{1}{2}, \frac{1}{2}, 0)$; the oblate limit (disk-like) has $(L_1, L_2, L_3) = (1, 0, 0)$.

3. CONTINUOUS DISTRIBUTIONS OF ELLIPSOIDS

3.1. Shape Factors

Every ellipsoidal shape is uniquely specified by its triplet of depolarization factors (L_1, L_2, L_3) . Consider a population of ellipsoidal grains, each with the same volume V , but with some continuous distribution of axial ratios – this is referred to as a “continuous distribution of ellipsoids” (CDE). Suppose that each grain has principal axes labelled 1,2,3 arbitrarily, and that $G(\ell_1, \ell_2) d\ell_1 d\ell_2$ is the fraction of the population with $L_1 \in [\ell_1, \ell_1 + d\ell_1]$, $L_2 \in [\ell_2, \ell_2 + d\ell_2]$, and $L_3 = 1 - L_1 - L_2$. The function G is non-negative ($G \geq 0$) and normalized: $\int G(L_1, L_2) dL_1 dL_2 = 1$ over the allowed (L_1, L_2) domain. If labels 1,2,3 were assigned arbitrarily, the function G must satisfy symmetry requirements, including $G(L_1, L_2) = G(L_2, L_1) = G(L_1, 1 - L_1 - L_2)$,¹ but otherwise we have no a-priori knowledge of the function G , other than expecting that very extreme axial ratios should be rare.

¹ One can also consider functions G that do not satisfy these symmetry requirements, but in this case one must restrict discussion to only one of the six subregions in Figure 1.

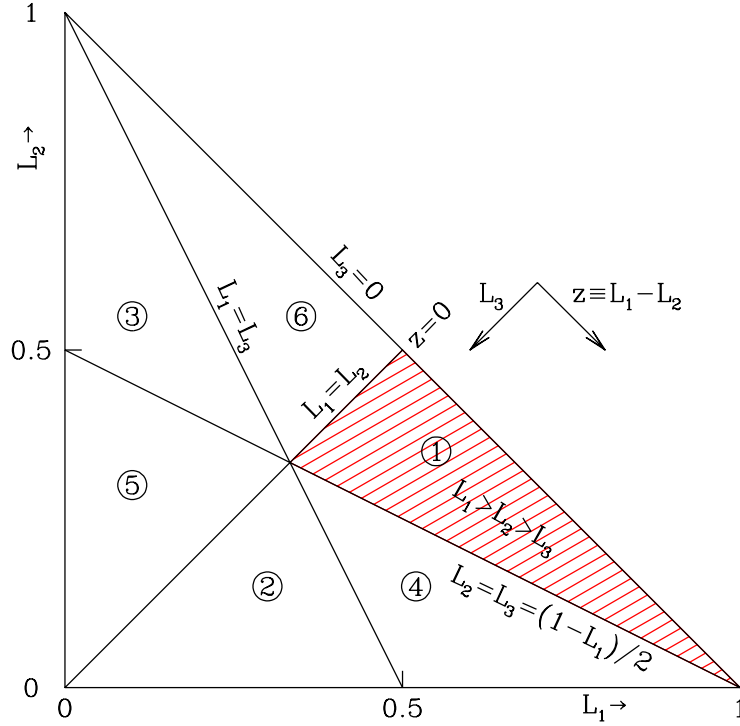


Figure 1. The domain of allowed shape factors (L_1, L_2) . The shaded region is the domain where $L_3 \leq L_2 \leq L_1$ (see text). Other regions, numbered 2-6, correspond to the other possible orderings of L_1, L_2, L_3 .

Various distributions of shapes have been considered in the literature, including spheroids (Treffers & Cohen 1974; Min et al. 2003), and ellipsoids (Bohren & Huffman 1983). Bohren & Huffman (1983) gave a lucid introduction to CDEs in general, and presented a simple illustrative example, referred to here as the BHCDE. We discuss the BHCDE and two other distributions of ellipsoids that have been considered in the astrophysical literature.

1. BHCDE: The simplest functional form

$$G(L_1, L_2) = 2 \quad \text{for } L_1 \geq 0, L_2 \geq 0, L_1 + L_2 \leq 1 \quad (20)$$

is often considered; Bohren & Huffman (1983) present this as an example, and it has subsequently been applied by a number of authors (e.g., Rouleau & Martin 1991; Alexander & Ferguson 1994; Min et al. 2003, 2006; Sargent et al. 2006; Min et al. 2008; Rho et al. 2018). Because $G(L_1, L_2)$ is independent of L_1 and L_2 , it is sometimes asserted that “all shapes are equally probable” (Bohren & Huffman 1983) or “all shapes are equally weighted” (Sargent et al. 2006), seemingly suggesting that this is a “fair” sampling of ellipsoidal shapes. While it is correct that all ellipsoidal shapes are present, it is not clear how “all shapes are equally probable” is to be understood, given that shapes are not discrete and there is no commonly accepted metric for “shape space”.

Although having the virtue of analytic simplicity, we will see below that the BHCDE distribution has an extreme representation of very elongated shapes, with $L \rightarrow 0$. We will argue that the BHCDE distribution seems unlikely to approximate grain shape distributions in nature, whether for desert sand or interstellar dust.

2. **ERCDE:** Zubko et al. (1996) proposed eliminating the most extreme shapes by truncating the distribution (20):

$$G(L_1, L_2) = \frac{2}{(1 - 3L_{\min})^2} \quad \text{for } L_1 \geq L_{\min}, L_2 \geq L_{\min}, L_1 + L_2 \leq 1 - L_{\min} \quad , \quad (21)$$

referring to this as the “externally-restricted CDE” (ERCDE). L_{\min} is a free parameter. While removing extreme shapes with $L_j \rightarrow 0$ or $L_j \rightarrow 1$ is desirable, the ERCDE distribution still seems unphysical, as we will see below. Note that if $L_{\min} \rightarrow 0$, the ERCDE \rightarrow BHCDE.

3. **CDE2:** Ossenkopf et al. (1992) proposed the distribution

$$G(L_1, L_2) = 120L_1L_2L_3 = 120L_1L_2(1 - L_1 - L_2) \quad \text{for } L_1 \geq 0, L_2 \geq 0, L_1 + L_2 \leq 1 \quad , \quad (22)$$

which has the desirable behavior $G \rightarrow 0$ for $L_3 \rightarrow 0$ and $L_1 \rightarrow 1$. This distribution has subsequently been referred to as “CDE2” (Fabian et al. 2001; Sargent et al. 2006), and we shall so refer to it here.

The distribution functions $G(L_1, L_2)$ for these three CDEs are shown in Figure 2.

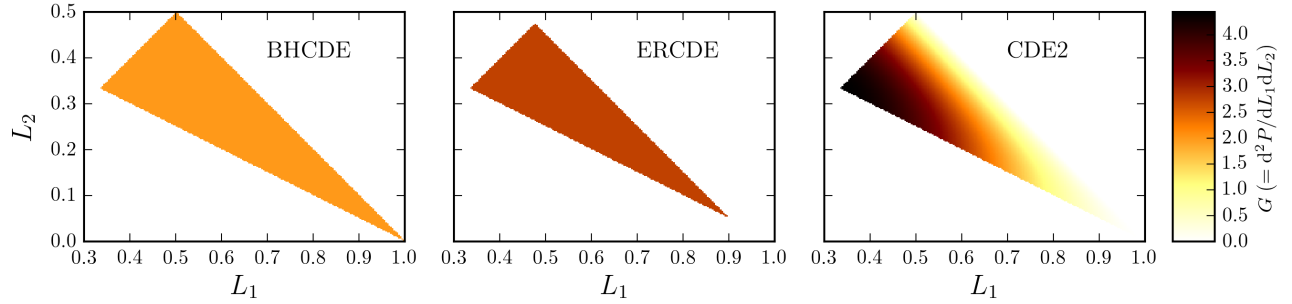


Figure 2. $G(L_1, L_2)$ for the BHCDE, ERCDE (with $L_{\min} = 0.05$) and CDE2 shape distributions.

3.2. Shape Distributions

Because the optical properties of ellipsoids in the limit $a \ll \lambda$ are determined by L_1 , L_2 , and $L_3 = 1 - L_1 - L_2$, most discussions of CDEs have been concerned only with the distribution of L_j values, rather than the distributions of the ellipsoid axial ratios. However, it is of interest to examine the distributions of actual grain shapes that correspond to the BHCDE, ERCDE, and CDE2 distributions.

For a given set of axial ratios $(a_2/a_1, a_3/a_1)$, the L_j values can be obtained by numerical quadrature [Eq. (2)]. Since there does not appear to be any direct way to invert Eq. (2) to obtain $(a_2/a_1, a_3/a_1)$ from given (L_1, L_2) , we have implemented a numerical procedure to find $(a_2/a_1, a_3/a_1)$ corresponding to given (L_1, L_2) . In Appendix D, we demonstrate that any solution found in this way is unique.

We continue to adopt the ordering $a_1 \leq a_2 \leq a_3$, $L_1 \geq L_2 \geq L_3$. We draw (L_1, L_2) values randomly according to the BHCDE, ERCDE, or CDE2 distributions, and for each (L_1, L_2) find the corresponding axial ratios $(a_2/a_1, a_3/a_1)$. Figure 3 shows 20 examples selected randomly from each of these shape distributions. Figure 4a shows the distribution of long/short axial ratios a_3/a_1 for the BHCDE, ERCDE (with $L_{\min} = 0.05$), and CDE2 distributions. Figure 4b shows the cumulative distribution function of axial ratios a_3/a_1 , and Figure 5 shows the distributions of axial ratios for the BHCDE, ERCDE, and CDE2 distributions. Some characteristics of these shape distributions are listed in Table 1.

The BHCDE distribution has a very large fraction of extreme axial ratios – Figure 4b shows that 10% of the realizations have $a_3/a_1 > 19.7$, and 1% of the realizations have $a_3/a_1 > 98.5$. Extreme elongation will

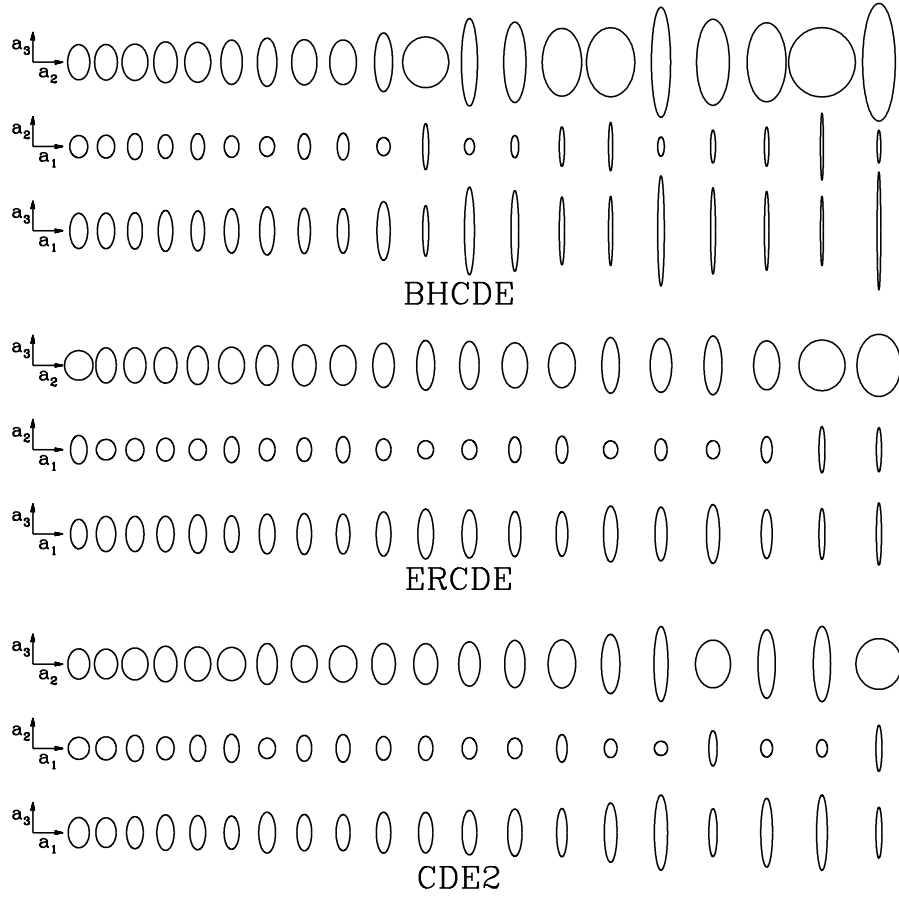


Figure 3. 20 randomly-selected ellipsoids drawn from the BHCDE, ERCDE, and CDE2 distributions. All examples have equal volume. 3 views are shown for each shape: viewed along the short axis \hat{a}_1 (top row), and along the \hat{a}_3 and \hat{a}_2 axes (2nd and 3rd rows). For each distribution the 20 random shapes are shown in order of increasing a_3/a_1 (left to right).

increase the susceptibility to fragmentation in high-speed grain-grain collisions. Highly elongated grains may also be more vulnerable to centrifugal disruption if spun-up by strong radiative torques (Silsbee & Draine 2016; Hoang 2019) or gas-grain streaming (e.g., Tatsuuma & Kataoka 2021). The actual shape distribution for interstellar grains is of course unknown, but it seems unlikely to include as large a fraction

Table 1. Long/Short Axis Ratio a_3/a_1

	BHCDE	ERCDE ^b	CDE2
mode ^a	3.26	3.27	2.24
median	4.58	3.35	2.73
25%	9.23	5.07	4.25
10%	19.7	6.97	6.72
5%	32.97	8.32	9.11
1%	98.49	10.92	17.11

^a Maximum of $dP/d\ln(a_3/a_1)$.

^b $L_{\min} = 0.05$.

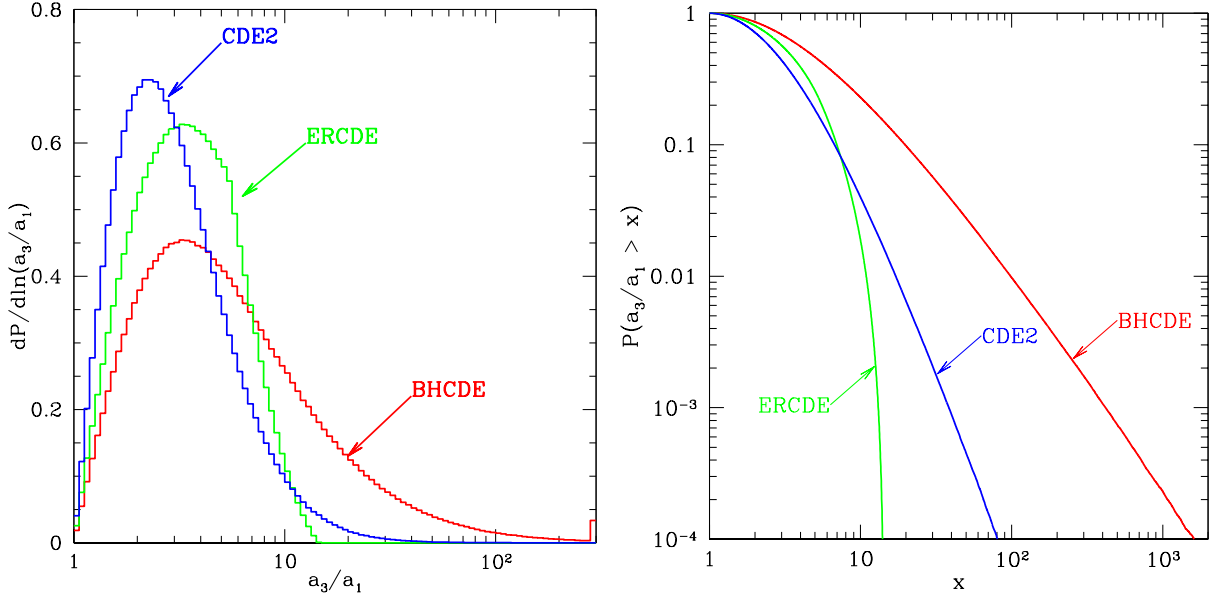


Figure 4. (a) Distribution of long/short axial ratio a_3/a_1 for three continuous distributions of ellipsoids. The ERCDE with $L_{\min} = 0.05$ has a maximum allowed axial ratio $a_3/a_1 = 14$, but the CDE2 and BHCDE distributions both extend to infinite axial ratios. The BHCDE distribution has a much larger representation of extreme axial ratios. (b) Cumulative distribution functions. For the BHCDE distribution, 10% of the realizations have $a_3/a_1 > 19.7$, and 1% have $a_3/a_1 > 98.5$.

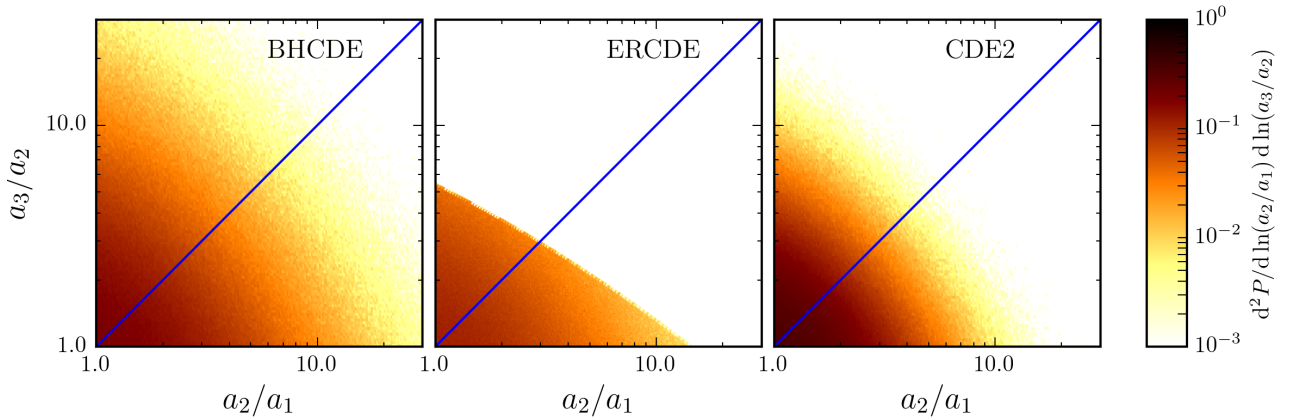


Figure 5. Distributions of axial ratios a_3/a_2 and a_2/a_1 for the BHCDE, ERCDE ($L_{\min} = 0.05$), and CDE2 shape distributions. Oblate spheroids have $a_3/a_2 = 1$, and prolate spheroids have $a_2/a_1 = 1$.

of extreme aspect ratios as the BHCDE distribution. The CDE2 (with $\sim 90\%$ of the draws having $a_3/a_1 < 6.72$) or ERCDE (with $\sim 90\%$ of the draws having $a_3/a_1 < 6.9$ for $L_{\min} = 0.05$) may be more plausible shape distributions to consider for interstellar dust grains.

4. POLARIZATION BY CDES

The observed polarization of starlight by dust, and of submm emission from dust in the interstellar medium, indicates that interstellar grains spin with their short axis tending to be aligned with the local magnetic field \mathbf{B} ; this occurs because the grain's angular momentum \mathbf{J} tends to align with the magnetic

field, and the short axis of the grain tends to align with \mathbf{J} . Rotation and nutation, and precession of \mathbf{J} around \mathbf{B} , are all rapid, and physical processes such as paramagnetic dissipation cause \mathbf{J} to align with \mathbf{B} .

In protoplanetary disks, magnetic effects are relatively much weaker. Grain drift can cause \mathbf{J} to tend to be perpendicular to the (azimuthal) streaming direction (Gold 1952), while radiative torques may cause \mathbf{J} to tend toward the radial direction (Lazarian & Hoang 2007; Tazaki et al. 2017). Whatever the spin-up process, if the grains are spinning suprathermally we expect dissipation in the grain to cause the short axis to be aligned with \mathbf{J} . The results obtained below for absorption cross sections averaged over CDEs are applicable both to the interstellar medium and to protoplanetary disks. This is true also for the polarization cross sections, provided only that the degree of alignment of the short axis with \mathbf{J} is independent of shape. Interpretation of observed polarization is often complicated by the need to include polarized scattering, which can even be important at submm wavelengths in protoplanetary disks (Kataoka et al. 2015).

In order to discuss polarization by a population of partially-aligned grains, we require the distribution of depolarization factors separately for the short axis, and for the other two axes.

It is useful to restrict consideration to the ordering $0 \leq L_3 \leq L_2 \leq L_1 \leq 1$: for each ellipsoid, $j = 3$ corresponds to the long axis, $j = 1$ to the short axis, and $j = 2$ to the intermediate axis. Let $g_j(\ell)d\ell$ be the fraction of ellipsoids with $L_j \in [\ell, \ell + d\ell]$. The distribution functions g_1, g_2, g_3 can be obtained from G , as discussed in Appendix A. Figure 6 shows g_1, g_2 , and g_3 for the BHCDE, ERCDE, and CDE2 shape distributions.

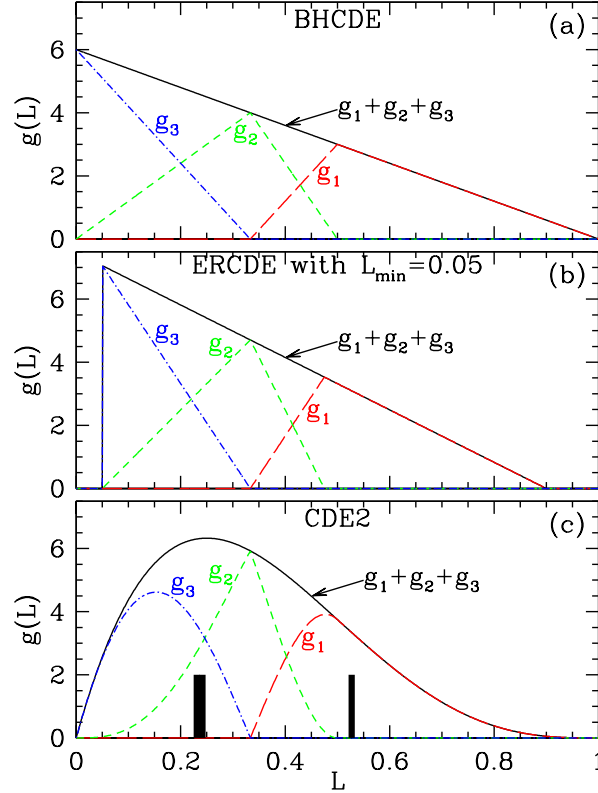


Figure 6. Distributions g_1, g_2 , and g_3 of depolarization factors L_1, L_2, L_3 for the three CDE distributions discussed in §3: (a) Bohren & Huffman CDE (BHCDE) from Eq. (20). (b) Externally-restricted CDE (ERCDE) from Eq. (21) with $L_{\min} = 0.05$. (c) Ossenkopf, Henning & Mathis CDE (CDE2) from Eq. (22). The BHCDE and ERCDE distributions have extreme representation of small L . Of the three, the CDE2 distribution appears most realistic (see text). The solid bars in panel (c) show the values of $L_3 = L_2 = 0.2364$ and $L_1 = 0.5272$ for a $b/a = 2$ oblate spheroid.

4.1. The BHCDE Distribution

Figure 6a shows the distribution functions g_j for the BHCDE distribution. We see that $g_3(\ell)$ peaks at $\ell = 0$, corresponding to infinitely elongated needles: fully 10% of the BHCDE ellipsoids have $L_3 < 0.0171$. Only very extreme shapes have such small values of L_3 – for example, a prolate spheroid with axial ratios 1 : 1 : 11.17 has $L_3 = 0.0171$. Another example with $L_3 = 0.0171$ would be an ellipsoid with axial ratios 1 : 4.72 : 22.3. It does not seem likely (to us) that interstellar grains will have such a large fraction of extremely elongated shapes.

4.2. The ERCDE Distribution

The ERCDE distribution is similar to the BHCDE distribution, except that cases with $L < L_{\min}$ are excluded. Thus L_{\min} is a free parameter for the ERCDE distribution. The ERCDE distribution has g_3 peaking at $L_3 = L_{\min}$. As an example, we consider $L_{\min} = 0.05$ (see Figure 6c).

What shapes would correspond to the limiting cases $L_3 = L_{\min}$? One example of a shape with $L_3 = 0.05$: a prolate spheroid with axial ratios 1 : 1 : 5.41 (with $L_1 = L_2 = 0.475$, $L_3 = 0.05$). Another example: an oblate spheroid with axial ratios 1 : 14.43 : 14.43 (with $L_1 = 0.9$, $L_2 = L_3 = 0.05$). A third example: an ellipsoid with axial ratios 1 : 2.965 : 8.79 (with $L_1 = 0.719$, $L_2 = 0.231$, $L_3 = 0.05$).

Because g_3 increases monotonically as $L_3 \rightarrow L_{\min}$ (see Figure 6c), this shape distribution places substantial weight on the most extreme allowed grain shapes. For instance, fully 10% of the ERCDE realizations with $L_{\min} = 0.05$ have $L_3 < 0.06454$. Thus the ERCDE shape distribution also appears to overrepresent extreme shapes, unless $L_{\min} \gtrsim 0.10$. The ERCDE shape distribution will be further discussed below.

4.3. The CDE2 Distribution

The distribution functions g_j for the CDE2 distribution are shown in Figure 6c. While the CDE2 does include extreme shapes, it has $g_3 \rightarrow 0$ for $L_3 \rightarrow 0$, and $g_1 \rightarrow 0$ for $L_1 \rightarrow 1$. 10% of the realizations have $L_3 < 0.06185$, so it is somewhat similar to the ERCDE with $L_{\min} = 0.05$ in the representation of extreme shapes, although the CDE2 distribution function has the virtue of smoothness.

5. ABSORPTION CROSS SECTIONS FOR THE BHCDE, ERCDE AND CDE2 DISTRIBUTIONS

The shape-averaged absorption cross section associated with axis j is

$$C_{\text{abs}}(\mathbf{E} \parallel \hat{\mathbf{a}}_j) = \frac{2\pi V}{\lambda} \text{Im}(\langle A_j \rangle) \quad (23)$$

$$\langle A_j \rangle \equiv \int A_j g_j(\ell) d\ell \quad , \quad (24)$$

where A_j is related to the complex dielectric function ϵ through Eq. (1). For ellipsoids with specified axial ratios $a_1 : a_2 : a_3$, the g_j are δ -functions. As seen above, for a population of ellipsoids with a continuous distribution of shapes, the g_j become continuous distribution functions (see Fig. 6). Min et al. (2006) show that a single particle with an irregular shape also has its absorption cross section given by Eq. (23) with continuous distribution functions g_j .

5.1. Randomly-Oriented Particles

For randomly-oriented particles, the absorption cross section is

$$C_{\text{ran}} = \frac{2\pi V}{\lambda} \text{Im} \left[\frac{\langle A_1 \rangle + \langle A_2 \rangle + \langle A_3 \rangle}{3} \right] \quad . \quad (25)$$

Bohren & Huffman (1983) obtained the absorption cross section for randomly-oriented grains with the BHCDE shape distribution:

$$\frac{C_{\text{ran}}^{\text{BHCDE}}}{V} = \frac{4\pi}{\lambda} \text{Im} \left[\left(\frac{1+x}{x} \right) \ln \epsilon \right] \quad , \quad (26)$$

where $x \equiv \epsilon - 1$. For the ERCDE [Eq. (21)] the absorption cross section for randomly-oriented grains was obtained by Zubko et al. (1996):

$$\frac{C_{\text{ran}}^{\text{ERCDE}}}{V} = \frac{4\pi}{\lambda} \frac{1}{(1 - 3L_{\min})^2} \text{Im} \left\{ \left(\frac{1}{x} + D \right) \ln \left[\frac{1 + xD}{1 + xL_{\min}} \right] \right\} , \quad (27)$$

where $D \equiv 1 - 2L_{\min}$. It is easily verified that this reduces to Eq. (26) for $L_{\min} \rightarrow 0$.

Fabian et al. (2001) obtained the absorption cross section for randomly-oriented ellipsoids with the CDE2 shape distribution [Eq. (22)]:

$$\frac{C_{\text{ran}}^{\text{CDE2}}}{V} = \frac{40\pi}{\lambda} \text{Im} \left[\frac{1}{x^4} \left(-(1+x)^3 \ln(1+x) + x + \frac{5}{2}x^2 + \frac{11}{6}x^3 + \frac{1}{4}x^4 \right) \right] . \quad (28)$$

5.2. Polarization Cross Sections for Aligned Particles

The polarization cross section (see Eq. 12) is

$$C_{\text{pol}} \equiv \frac{\pi V}{\lambda} \text{Im} \left[\frac{\langle A_2 \rangle + \langle A_3 \rangle - 2\langle A_1 \rangle}{2} \right] . \quad (29)$$

For the BHCDE distribution, we find

$$\begin{aligned} \frac{C_{\text{pol}}^{\text{BHCDE}}}{V} = \frac{3\pi}{2\lambda} \text{Im} & \left[\frac{12}{x} \left(1 + \frac{x}{2} \right) \ln \left(1 + \frac{x}{2} \right) - \frac{9}{x} \left(1 + \frac{x}{3} \right) \ln \left(1 + \frac{x}{3} \right) \right. \\ & \left. - \frac{2}{x} (1+x) \ln(1+x) \right] . \end{aligned} \quad (30)$$

where $x \equiv \epsilon - 1$. For the ERCDE distribution we find

$$\begin{aligned} \frac{C_{\text{pol}}^{\text{ERCDE}}}{V} = \frac{3\pi}{2\lambda} \frac{1}{(1 - 3L_{\min})^2} \text{Im} & \left\{ 12 \left(\frac{1}{x} + B \right) \ln [1 + xB] - 9 \left(\frac{1}{x} + \frac{1}{3} \right) \ln \left[1 + \frac{x}{3} \right] \right. \\ & \left. - \left(\frac{1}{x} + D \right) \ln [1 + xL_{\min}] - 2 \left(\frac{1}{x} + D \right) \ln [1 + xD] \right\} \end{aligned} \quad (31)$$

$$B \equiv \frac{1}{2} - \frac{L_{\min}}{2} , \quad D \equiv 1 - 2L_{\min} . \quad (32)$$

See Appendix A for the derivation of Eq. (31). Eq. (30) is recovered by setting $L_{\min} = 0$.

The polarization cross section for the CDE2 distribution is (see Appendix A):

$$\begin{aligned} \frac{C_{\text{pol}}^{\text{CDE2}}}{V} = \frac{30\pi}{\lambda} \text{Im} & \left[\frac{1}{x^4} \left(3(-9 - 3x + 3x^2 + x^3) \ln \left(1 + \frac{x}{3} \right) + 6(4 - 3x^2 - x^3) \ln \left(1 + \frac{x}{2} \right) \right. \right. \\ & \left. \left. + 2(1+x)^3 \ln(1+x) - 5x - \frac{1}{2}x^2 + \frac{7}{6}x^3 + \frac{11}{72}x^4 \right) \right] . \end{aligned} \quad (33)$$

6. POLARIZED ABSORPTION BY PARTIALLY-ALIGNED GRAINS

An interstellar grain with angular momentum \mathbf{J} will have a magnetic moment $\boldsymbol{\mu}$ resulting from a combination of the Barnett effect (if the grain has unpaired electron spins), the Rowland effect (if the grain is charged), and ferromagnetism (if the grain contains magnetic material).² If $|\mathbf{J} \times \mathbf{B}| \neq 0$, the $\boldsymbol{\mu} \times \mathbf{B}_0$ torque will cause \mathbf{J} to precess around \mathbf{B}_0 . There are three distinct orientational issues:

² For ferromagnetic grains, the rotation-averaged effective magnetic moment $\langle \boldsymbol{\mu} \rangle = \mathbf{J} \langle \mathbf{J} \cdot \boldsymbol{\mu} \rangle / J^2$.

1. The angle α between the grain's principal axis of largest moment of inertia, $\hat{\mathbf{a}}_1$, and the angular momentum \mathbf{J} (alignment of the grain body with \mathbf{J}).
2. The angle β between \mathbf{J} and \mathbf{B}_0 (alignment of \mathbf{J} with \mathbf{B}_0).
3. The angle γ between \mathbf{B}_0 and the line-of-sight.

Consider radiation propagating in the $\hat{\mathbf{z}}$ direction, and suppose \mathbf{B}_0 to be in the $\hat{\mathbf{y}}\text{-}\hat{\mathbf{z}}$ plane, making an angle γ with the $\hat{\mathbf{z}}$ axis. In the electric-dipole limit $a/\lambda \ll 1$, the mean absorption cross section and the polarization cross section sections for x - and y -polarized radiation can be written (see Appendix B)

$$\frac{C_x + C_y}{2} = C_{\text{ran}} - C_{\text{pol}} \Phi \left(\sin^2 \gamma - \frac{2}{3} \right) \quad (34)$$

$$\frac{C_x - C_y}{2} = C_{\text{pol}} \Phi \sin^2 \gamma \quad , \quad (35)$$

where (see Appendix B)

$$\Phi \equiv \frac{9}{4} \left(\langle \cos^2 \alpha \rangle - \frac{1}{3} \right) \left(\langle \cos^2 \beta \rangle - \frac{1}{3} \right) \quad (36)$$

is a generalization of the ‘‘polarization reduction factor’’ originally introduced by [Greenberg \(1968, p. 328\)](#) and [Purcell & Spitzer \(1971\)](#). Perfect alignment ($\langle \cos^2 \alpha \rangle = \langle \cos^2 \beta \rangle = 1$) has $\Phi = 1$; random orientation ($\langle \cos^2 \beta \rangle = 1/3$) results in $\Phi = 0$.

If \mathbf{B}_0 is itself not perfectly uniform, [Lee & Draine \(1985\)](#) showed that $\sin^2 \gamma \rightarrow \sin^2 \gamma_0 \times \frac{3}{2} (\langle \cos^2 \delta \rangle - \frac{1}{3})$ where γ_0 is now the angle between $\hat{\mathbf{z}}$ and the (dust mass-weighted) mean magnetic field $\langle \mathbf{B}_0 \rangle$, and δ is the angle between $\langle \mathbf{B}_0 \rangle$ and the local \mathbf{B}_0 ; $\langle \cos^2 \delta \rangle$ is the dust mass-weighted average of $\cos^2 \delta$ over the sightline. If we assume that α , β and δ vary independently, then the overall polarization reduction factor becomes

$$\Phi \equiv \frac{27}{8} \left(\langle \cos^2 \alpha \rangle - \frac{1}{3} \right) \left(\langle \cos^2 \beta \rangle - \frac{1}{3} \right) \left(\langle \cos^2 \delta \rangle - \frac{1}{3} \right) \quad . \quad (37)$$

Let N_d be the column density of grains, and C_x and C_y be the average absorption cross section per grain for radiation polarized in the $\hat{\mathbf{x}}$ and $\hat{\mathbf{y}}$ directions. Let $\tau_x = N_d C_x$ and $\tau_y = N_d C_y$ be the optical depths for radiation polarized in the $\hat{\mathbf{x}}$ and $\hat{\mathbf{y}}$ directions. Initially unpolarized radiation will be attenuated and polarized as a result of linear dichroism (i.e., preferential attenuation of one linear polarization), with overall attenuation and fractional polarization

$$I/I_0 = \frac{e^{-\tau_y} + e^{-\tau_x}}{2} \quad (38)$$

$$p = \frac{e^{-\tau_y} - e^{-\tau_x}}{e^{-\tau_y} + e^{-\tau_x}} \quad . \quad (39)$$

From (34) and (35) we can find the absorption cross section per grain volume $C_{\text{ran}}(\lambda)/V$ from the measured attenuation I/I_0 and polarization p (see Appendix C) where ρ is the mass density of the grain material, and Σ_d is the dust mass surface density:

$$\frac{C_{\text{ran}}(\lambda)}{V} = \frac{\tau_\lambda}{\Sigma_d/\rho} \left[1 + \frac{p_\lambda}{\tau_\lambda} \left(1 - \frac{2}{3 \sin^2 \gamma} \right) - \frac{p_\lambda^2}{2\tau_\lambda} - \frac{2p_\lambda^3}{3\tau_\lambda} \left(1 - \frac{2}{3 \sin^2 \gamma} \right) + O \left(\frac{p_\lambda^4}{\tau_\lambda} \right) \right] \quad (40)$$

$$\tau_\lambda \equiv \ln(I_0/I) \quad . \quad (41)$$

Because p_λ/τ_λ is normally small, common practice is to approximate $C_{\text{ran}}(\lambda)/V \approx \tau_\lambda/(\Sigma_d/\rho)$; note, however, that [Hensley et al. \(2019\)](#) have demonstrated that the high quality of the *Planck* data permit the dependence of the total emission on p_λ/τ_λ (the first-order term in Eq. 40) to be used to constrain the full 3D orientation of the magnetic field.

7. SELF-CONSISTENT DIELECTRIC FUNCTIONS DERIVED FROM INFRARED ABSORPTION

The relationship between $C_{\text{abs}}(\lambda)$ and $C_{\text{pol}}(\lambda)$ derived in the previous sections can be leveraged on astronomical data in the infrared. Here we show how the full dielectric function $\epsilon(\lambda)$ can be estimated using knowledge of the infrared opacity.

Suppose that we have an estimate of the dielectric function $\epsilon(\lambda)$ of the grain material at short wavelengths $\lambda < \lambda_1$, and have observational knowledge of the extinction $\tau(\lambda)$ at infrared wavelengths $\lambda > \lambda_1$, Σ_d , and an estimate for the grain material density ρ . From these we can estimate the observed absorption cross section per grain volume $C_{\text{ran}}^{(\text{obs})}/V$ for randomly-oriented grains (see Appendix C). This applies to the dust material in the ISM, where we have constraints on the infrared and far-infrared opacity, including the strong silicate absorption features at $9.7\mu\text{m}$ and $18\mu\text{m}$. Here we show how one can use the “observed” $C_{\text{ran}}^{(\text{obs})}(\lambda)/V$ to obtain the complex dielectric function $\epsilon(\lambda)$ at infrared wavelengths.

We assume that at wavelengths $\lambda > \lambda_1$ the grains have $a \ll \lambda$, so that we can employ the electric dipole approximation (8) to relate C_{ran}/V to the complex dielectric function. We must, of course, make an assumption about the grain shape, or distribution of grain shapes. For spheres, spheroids, ellipsoids, or the CDEs discussed in this paper, we have analytic expressions relating C_{ran}/V to the dielectric function $\epsilon(\lambda)$; the analytic result enables efficient iterative algorithms to be applied to solve the system of equations.

The dielectric function must satisfy the Kramers-Kronig relations (Landau et al. 1993). We suppose that we start with a dielectric function $\epsilon^0(\lambda)$ that is reasonably accurate at $\lambda < \lambda_1$. We extend the imaginary part of ϵ^0 to long wavelengths in a smooth way:

$$\epsilon_2^0(\lambda) = \epsilon_2^0(\lambda_1) \times \left(\frac{\lambda_1}{\lambda} \right) \quad , \quad (42)$$

and obtain (by numerical integration) the real part $\epsilon_1^0(\lambda)$ at all wavelengths using the Kramers-Kronig relation (Landau et al. 1993):

$$\epsilon_1^0(\omega) = 1 + \frac{2}{\pi} P \int_0^\infty \frac{x \epsilon_2^0(x)}{x^2 - \omega^2} dx \quad , \quad (43)$$

where P indicates that the “principal value” of the singular integral is to be taken. The actual behavior of $\epsilon_2^0(\lambda > 1\mu\text{m})$ is unimportant, because we will adjust the total absorption as required to reproduce $C_{\text{ran}}^{(\text{obs})}/V$ at $\lambda > \lambda_1$. We accomplish this by adding additional absorption in the form of N Lorentz oscillators, each with resonant frequency ω_{0k} , dimensionless damping parameter γ_k , and dimensionless strength S_k :

$$\epsilon(\omega) = \epsilon^{(0)}(\omega) + \sum_{k=1}^N S_k \left[1 - \left(\frac{\omega}{\omega_{0k}} \right)^2 - i \gamma_k \frac{\omega}{\omega_{0k}} \right]^{-1} \quad . \quad (44)$$

Because $\epsilon^{(0)}(\omega)$ and each of the Lorentz oscillators separately satisfy the Kramers-Kronig relations, $\epsilon(\omega)$ given by Eq. (44) will satisfy the Kramers-Kronig relations for any $\{\omega_{0k}, \gamma_k, S_k\}$.

We distribute the Lorentz oscillators between λ_1 and $\lambda_N > \lambda_1$ according to some smooth prescription (e.g., uniform in $\log \lambda$). Then, we set the widths of the Lorentzians by specifying the dimensionless damping parameters γ_k :

$$\gamma_k = C \times \left(\frac{\lambda_j}{\lambda_{j-1}} - 1 \right) \quad \text{with } j = \min(2, k) \quad . \quad (45)$$

For $\gamma_k \ll 1$, each resonance contributes $\text{Im}(\epsilon)$ with a FWHM $\approx \gamma_k \omega_{0k}$. To represent a smooth function, we want $\gamma_k \omega_{0k}$ to be large compared to $\omega_{0,k+1} - \omega_{0k}$, but small enough to be able to reproduce the expected frequency dependence of $\text{Im}(\epsilon)$. This is accomplished by suitable choice for C . For example, Draine & Hensley (2021) adopt $N = 3000$, $\omega_{01}/\omega_{0N} = 3 \text{ cm}/1\mu\text{m} = 3 \times 10^4$, and $C = 10$.

The model cross sections $C_{\text{ran}}^{(\text{model})}(\lambda)$ depend on the $\{S_k\}$. To find the self-consistent solution, we iteratively adjust the S_k to solve the N simultaneous equations

$$Y_k \equiv \left[\frac{\lambda C_{\text{ran}}^{(\text{model})}}{V} \right]_{\lambda_k} - \left[\frac{\lambda C_{\text{ran}}^{(\text{obs})}}{V} \right]_{\lambda_k} = 0 \quad , \quad k = 1, \dots, N \quad . \quad (46)$$

Thus we have N equations to determine N unknown S_k . Iterative algorithms, such as the Levenberg-Marquardt method (see, e.g., [Press et al. 1992](#)), can be used to find the solution S_k ; it is helpful that analytic formulae for the partial derivatives $\partial Y_j / \partial S_k$ can be obtained from Eq. (44) and one of (26), (27), or (28).

We remark here that the problem does not always have a solution: if the “observed” $\lambda C_{\text{ran}}^{(\text{obs})} / V$ is too large, there may not be any dielectric function $\epsilon(\lambda)$ that can reproduce the assumed $\lambda C_{\text{ran}}^{(\text{obs})} / V$ for the assumed grain shape. Because of the Kramers-Kronig relations, all wavelengths matter: strong absorption at one wavelength will imply a large $\text{Re}(\epsilon)$ at longer wavelengths, limiting the ability of the grain to absorb at those wavelengths.

We apply this methodology to estimate the effective dielectric function $\epsilon(\lambda)$ for interstellar dust material in a separate paper ([Draine & Hensley 2021](#)).

8. ELLIPSOIDS VS. MORE COMPLEX SHAPES

This paper has concentrated on the optics of grains with spheroidal or ellipsoidal shapes, including continuous distributions of ellipsoidal shapes. In the Rayleigh limit $a \ll \lambda$, the interaction of a grain with the electromagnetic field is determined by a single symmetric tensor α_{jk} characterizing the polarizability of the grain. For a given dielectric function, ellipsoidal shapes allow us to explore plausible values for α_{jk} / V .

At shorter wavelengths, the response of the grain to an incident electromagnetic field is more complex, and ellipsoidal shapes provide only a first approximation to asphericity. Ellipsoidal shapes may be an adequate approximation for estimation of cross sections for absorbing or scattering light, for modeling polarization of starlight at optical wavelengths, or polarized thermal emission at submm wavelengths.

However, radiative torques are important for grain dynamics, including the alignment of interstellar grains ([Draine & Weingartner 1996, 1997](#); [Hoang & Lazarian 2008](#)). The reflection symmetries (and therefore zero chirality) of ellipsoidal shapes artificially suppresses radiative torques. Therefore, studies of radiative torques on interstellar grains must consider non-ellipsoidal grain shapes. However, the overall deviations from nonsphericity implied by observations of polarized emission at long wavelengths will still serve to constrain the more complex shapes used for studies of starlight torques.

9. SUMMARY

The principal results of this study are as follows:

1. We discuss the distributions of ellipsoidal shapes that correspond to three previously-proposed continuous distributions of ellipsoids (CDEs). Twenty randomly-selected shapes from each distribution (Figure 3) serve to illustrate the three distributions.
2. The often-used CDE discussed by [Bohren & Huffman \(1983\)](#) (here referred to as the BHCDE distribution) includes what appears to be an unrealistically large fraction of extremely elongated or extremely flattened shapes.
3. The CDE2 distribution proposed by [Ossenkopf et al. \(1992\)](#) includes a much smaller fraction of extreme shapes, and seems more realistic as a model for distributions of grain shapes.
4. For each of the three CDEs considered here, we obtain the distribution functions $g_j(L_j)$ for the geometric factors L_1, L_2, L_3 .
5. In the electric dipole limit $a/\lambda \ll 1$, we obtain absorption and polarization cross sections for partially-aligned ellipsoidal grains with the three proposed CDEs.

6. We present a method for obtaining a self-consistent dielectric function consistent with an assumed absorption opacity and an assumed distribution of shapes.

ACKNOWLEDGMENTS

We thank Eric Stansifer and Chris Wright for helpful discussions. We thank the referee for helpful comments, and also thank a previous referee for comments on an earlier version. This work was supported in part by NSF grants AST-1408723 and AST-1908123, and carried out in part at the Jet Propulsion Laboratory, California Institute of Technology, under a contract with the National Aeronautics and Space Administration.

APPENDIX

A. POLARIZATION CROSS SECTIONS FOR GRAIN POPULATIONS WITH CONTINUOUSLY-DISTRIBUTED ELLIPTICITIES

A.1. General Considerations

Consider a population of ellipsoids with a distribution of axial ratios. Every ellipsoidal shape is uniquely specified by its triplet of depolarization factors (L_1, L_2, L_3) . Because $L_3 = 1 - L_1 - L_2$, the ellipsoid is fully-determined by the doublet (L_1, L_2) , which must lie in the triangular region bounded by $L_1 = 0$, $L_2 = 0$, and $L_1 + L_2 = 1$, as shown in Figure 1.

The distribution of shapes can be characterized by the distribution of L values. Let $dP = G(L_1, L_2)dL_1dL_2$ be the probability that $L_1 \in (L_1 + dL_1)$, $L_2 \in (L_2 + dL_2)$. The function $G(L_1, L_2)$ fully determines the shape distribution (i.e., the distribution of axial ratios). If G is to apply to the full triangular region in Figure 1, then (because labelling of axes 1, 2, 3 is arbitrary), G must depend symmetrically on L_1, L_2, L_3 :

$$G(L_1, L_2) = G(L_2, L_1) = G(L_1, 1 - L_1 - L_2) \text{ for all allowed } L_1, L_2. \quad (\text{A1})$$

The region of allowed (L_1, L_2) can be divided into 6 triangular subregions of equal area, shown in Figure 1, corresponding to the six possible orderings of L_1, L_2, L_3 : (1) $L_3 \leq L_2 \leq L_1$, (2) $L_2 \leq L_1 \leq L_3$, (3) $L_1 \leq L_3 \leq L_2$, (4) $L_2 \leq L_3 \leq L_1$, (5) $L_3 \leq L_1 \leq L_2$, and (6) $L_1 \leq L_2 \leq L_3$.

For clarity, we fix the order of the L values: we choose the ordering $0 \leq L_3 \leq L_2 \leq L_1 \leq 1$, corresponding to region 1 (shaded) in Figure 1. Then L_1 is for \mathbf{E} parallel to the principal axis of largest moment of inertia (the “short axis”), and L_3 is for \mathbf{E} along the principal axis of smallest moment of inertia (the “long axis”).

Within subregion 1, let $g_j(L_j)dL_j$ be the probability that $L_j \in (L_j, L_j + dL_j)$:

$$\begin{aligned} g_1(L_1) &= 0 && \text{for } 0 < L_1 < 1/3 \\ &= 6 \int_{(1-L_1)/2}^{L_1} G(L_1, L_2)dL_2 && \text{for } 1/3 < L_1 < 1/2 \\ &= 6 \int_{(1-L_1)/2}^{1-L_1} G(L_1, L_2)dL_2 && \text{for } 1/2 < L_1 < 1 \\ g_2(L_2) &= 6 \int_{1-2L_2}^{1-L_2} G(L_1, L_2)dL_1 && \text{for } 0 < L_2 < 1/3 \\ &= 6 \int_{L_2}^{1-L_2} G(L_1, L_2)dL_1 && \text{for } 1/3 < L_2 < 1/2 \\ &= 0 && \text{for } 1/2 < L_2 \\ g_3(L_3) &= 3 \int_0^{1-3L_3} G((1-L_3+z)/2, (1-L_3-z)/2)dz && \text{for } 0 < L_3 < 1/3 \\ &= 0 && \text{for } 1/3 < L_3 \end{aligned} \quad (\text{A2})$$

where we have introduced $z \equiv (L_1 - L_2)$ for evaluation of g_3 . The factor of six in (A2) appears because we assume the normalization $\int G dL_1 dL_2 = 1$ over the full triangular region, hence $\int G dL_1 dL_2 = 1/6$ over

region 1. It can be verified that

$$\int_0^1 g_j(L_j) dL_j = 1 \quad \text{for } j = 1, 2, 3 \quad . \quad (\text{A3})$$

For distributions of ellipsoidal shapes,

$$\langle A_j \rangle \equiv \int \frac{(\epsilon - 1)}{1 + L_j(\epsilon - 1)} g_j(L_j) dL_j \quad . \quad (\text{A4})$$

A.2. BHCDE

The simplest CDE is the uniform distribution

$$G(L_1, L_2) = 2 \quad \text{for } 0 \leq L_1 + L_2 \leq 1 \quad , \quad (\text{A5})$$

which obviously satisfies the symmetry condition (A1). This example was discussed by [Bohren & Huffman \(1983\)](#); we refer to (A5) as the BHCDE. For this case we have

$$\begin{aligned} g_1 &= 0 && \text{for } L_1 < \frac{1}{3} \\ &= 18(L_1 - \frac{1}{3}) && \text{for } \frac{1}{3} \leq L_1 \leq \frac{1}{2} \\ &= 6(1 - L_1) && \text{for } \frac{1}{2} \leq L_1 \leq 1 \\ g_2 &= 12L_2 && \text{for } 0 \leq L_2 \leq \frac{1}{3} \\ &= 12(1 - 2L_2) && \text{for } \frac{1}{3} \leq L_2 \leq \frac{1}{2} \\ &= 0 && \text{for } \frac{1}{2} \leq L_2 \\ g_3 &= 6(1 - 3L_3) && \text{for } 0 \leq L_3 \leq \frac{1}{3} \\ &= 0 && \text{for } \frac{1}{3} \leq L_3 \quad . \end{aligned} \quad (\text{A6})$$

Distributions g_1 , g_2 , and g_3 are shown in Figure 6a. Then

$$\langle A_1 \rangle = \frac{6}{x} \left\{ (1+x) \ln \left(\frac{1+x}{1+x/2} \right) - 3 \left(1 + \frac{x}{3} \right) \ln \left(\frac{1+x/2}{1+x/3} \right) \right\} \quad (\text{A7})$$

$$\langle A_2 \rangle = \frac{12}{x} \left\{ 2 \left(1 + \frac{x}{2} \right) \ln \left(\frac{1+x/2}{1+x/3} \right) - \ln(1+x/3) \right\} \quad (\text{A8})$$

$$\langle A_3 \rangle = \frac{18}{x} \left\{ \left(1 + \frac{x}{3} \right) \ln(1+x/3) - \frac{x}{3} \right\} \quad . \quad (\text{A9})$$

$$\frac{\langle A_1 + A_2 + A_3 \rangle}{3} = \frac{2}{x} (1+x) \ln(1+x) - 2 \quad . \quad (\text{A10})$$

Eq. (A10) was previously obtained by [Bohren & Huffman \(1983\)](#).

A.3. ERCDE

The BHCDE includes shapes that are infinitely elongated ($L_j \rightarrow 0$) and infinitely flattened ($L_j \rightarrow 1$). [Zubko et al. \(1996\)](#) proposed to exclude the most extreme shapes by imposing the restriction $L_j \geq L_{\min}$, where $0 \leq L_{\min} \leq 1/3$, giving what Zubko et al. referred to as the “externally restricted distribution of ellipsoids” (ERCDE):

$$\begin{aligned} G(L_1, L_2) &= \frac{2}{(1 - 3L_{\min})^2} \quad \text{for} \\ &L_{\min} \leq L_1, L_{\min} \leq L_2, (L_1 + L_2) \leq 1 - 2L_{\min} \quad . \end{aligned} \quad (\text{A11})$$

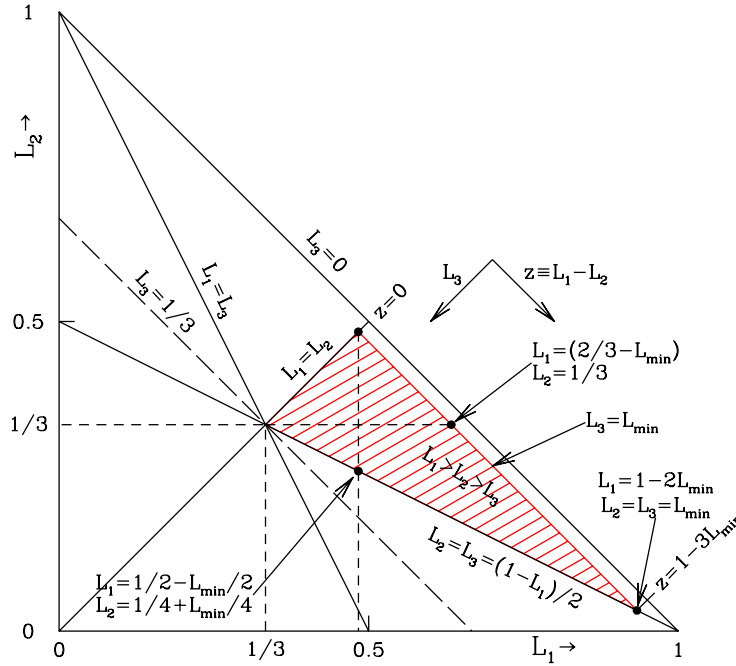


Figure 7. The shaded area is the ERCDE locus with depolarization factors $L_1 \geq L_2 \geq L_3 \geq L_{\min}$ (see text).

With $L_{\min} = 0$ one obtains the original BHCDE; with $L_{\min} \rightarrow 1/3$ one obtains spheres. The domain in the L_1 - L_2 plane is shown in Fig. 7.

Zubko et al. (1996) obtained $\langle A_1 + A_2 + A_3 \rangle$ for randomly-oriented grains with the ERCDE distribution. Discussion of aligned grains requires the absorption per volume for grains aligned with the electric fields along their principal axes. The ERCDE has

$$\begin{aligned}
 g_1 &= 0 && \text{for } L_1 < \frac{1}{3} \\
 &= \frac{18}{(1-3L_{\min})^2} \left(L_1 - \frac{1}{3} \right) && \text{for } \frac{1}{3} \leq L_1 \leq \frac{(1-L_{\min})}{2} \\
 &= \frac{6}{(1-3L_{\min})^2} (1 - L_1 - 2L_{\min}) && \text{for } \frac{(1-L_{\min})}{2} \leq L_1 \leq 1 - 2L_{\min} \\
 &= 0 && \text{for } 1 - 2L_{\min} \leq L_1 \\
 g_2 &= 0 && \text{for } L_2 < L_{\min} \\
 &= \frac{12}{(1-3L_{\min})^2} (L_2 - L_{\min}) && \text{for } L_{\min} \leq L_2 \leq \frac{1}{3} \\
 &= \frac{12}{(1-3L_{\min})^2} (1 - L_{\min} - 2L_2) && \text{for } \frac{1}{3} \leq L_2 \leq \frac{(1-L_{\min})}{2} \\
 &= 0 && \text{for } \frac{(1-L_{\min})}{2} \leq L_2 \\
 g_3 &= 0 && \text{for } L_3 \leq L_{\min} \\
 &= \frac{6}{(1-3L_{\min})^2} (1 - 3L_3) && \text{for } L_{\min} \leq L_3 \leq \frac{1}{3} \\
 &= 0 && \text{for } \frac{1}{3} \leq L_3 .
 \end{aligned} \tag{A12}$$

Distributions g_1 , g_2 , and g_3 are shown in Figure 6b for $L_{\min} = 0.05$. It is convenient to define

$$B \equiv 1/2 - L_{\min}/2 \tag{A13}$$

$$D \equiv 1 - 2L_{\min} \tag{A14}$$

$$x \equiv \epsilon - 1 . \tag{A15}$$

We obtain

$$\langle A_1 \rangle = \frac{6}{(1 - 3L_{\min})^2} \left\{ \left(\frac{1}{x} + D \right) \ln \left[\frac{1 + xD}{1 + xB} \right] - 3 \left(\frac{1}{x} + \frac{1}{3} \right) \ln \left[\frac{1 + xB}{1 + x/3} \right] \right\} \quad (\text{A16})$$

$$\langle A_2 \rangle = \frac{12}{(1 - 3L_{\min})^2} \left\{ 2 \left(\frac{1}{x} + B \right) \ln \left[\frac{1 + xB}{1 + x/3} \right] - \left(\frac{1}{x} + L_{\min} \right) \ln \left[\frac{1 + x/3}{1 + xL_{\min}} \right] \right\} \quad (\text{A17})$$

$$\langle A_3 \rangle = \frac{18}{(1 - 3L_{\min})^2} \left\{ \left(\frac{1}{x} + \frac{1}{3} \right) \ln \left[\frac{1 + x/3}{1 + xL_{\min}} \right] - \frac{(1 - 3L_{\min})}{3} \right\} \quad (\text{A18})$$

$$\frac{\langle A_1 + A_2 + A_3 \rangle}{3} = \frac{2}{(1 - 3L_{\min})^2} \left\{ \left(\frac{1}{x} + D \right) \ln \left[\frac{1 + xD}{1 + xL_{\min}} \right] - (1 - 3L_{\min}) \right\}. \quad (\text{A19})$$

Eq. (A19) was previously obtained by [Zubko et al. \(1996\)](#).

A.4. CDE2

[Ossenkopf et al. \(1992\)](#) proposed the distribution

$$G(L_1, L_2) = 120L_1L_2L_3 \quad . \quad (\text{A20})$$

This satisfies the symmetry requirement (A1), and has the desirable property that $G \rightarrow 0$ for $L_j \rightarrow 0$. We find

$$\begin{aligned} g_1(L_1) &= 0 && \text{for } L_1 < \frac{1}{3} \\ &= 60L_1(-1 + 3L_1 + 3L_1^2 - 9L_1^3) && \text{for } \frac{1}{3} \leq L_1 \leq \frac{1}{2} \\ &= 60L_1(1 - L_1)^3 && \text{for } \frac{1}{2} \leq L_1 \leq 1 \\ g_2(L_2) &= 120L_2^3(3 - 5L_2) && \text{for } 0 \leq L_2 \leq \frac{1}{3} \\ &= 120(L_2 - 3L_2^2 + 4L_2^4) && \text{for } \frac{1}{3} \leq L_2 \leq \frac{1}{2} \\ &= 0 && \text{for } \frac{1}{2} < L_2 \\ g_3(L_3) &= 60L_3(1 - 3L_3 - 3L_3^2 + 9L_3^3) && \text{for } 0 \leq L_3 \leq \frac{1}{3} \\ &= 0 && \text{for } \frac{1}{3} < L_3 \quad . \end{aligned} \quad (\text{A21})$$

These distributions are shown in Figure 6c. To have a sense of how nonspherical a typical ellipsoid from this distribution might be, we consider the mean depolarization factors $\langle L_j \rangle \equiv \int L_j g_j(L_j) dL_j$. For g_j given by eq. (A21) we find $\langle L_1 \rangle = 0.5355$, $\langle L_2 \rangle = 0.3040$, and $\langle L_3 \rangle = 0.1605$. These mean values correspond to an ellipsoid with axial ratios $a_1 : a_2 : a_3 :: 1 : 1.664 : 2.716$.

For g_j given by eq. (A21) we obtain

$$\begin{aligned} \langle A_1 \rangle &= \frac{60}{x^4} \left[(9 + 3x - 3x^2 - x^3) \ln \left(1 + \frac{x}{3} \right) + (-8 + 6x^2 + 2x^3) \ln \left(1 + \frac{x}{2} \right) \right. \\ &\quad \left. + (-1 - 3x - 3x^2 - x^3) \ln(1 + x) + 2x + x^2 + \frac{2}{9}x^3 + \frac{7}{216}x^4 \right] \quad (\text{A22}) \end{aligned}$$

$$\begin{aligned} \langle A_2 \rangle &= \frac{60}{x^4} \left[(-18 - 6x + 6x^2 + 2x^3) \ln \left(1 + \frac{x}{3} \right) + (8 - 6x^2 - 2x^3) \ln \left(1 + \frac{x}{2} \right) \right. \\ &\quad \left. + 2x + 2x^2 + \frac{5}{9}x^3 + \frac{13}{216}x^4 \right] \quad (\text{A23}) \end{aligned}$$

$$\langle A_3 \rangle = \frac{60}{x^4} \left[(9 + 3x - 3x^2 - x^3) \ln \left(1 + \frac{x}{3} \right) - 3x - \frac{1}{2}x^2 + \frac{19}{18}x^3 + \frac{17}{108}x^4 \right] \quad (\text{A24})$$

$$\frac{\langle A_1 + A_2 + A_3 \rangle}{3} = \frac{20}{x^4} \left[-(1 + x)^3 \ln(1 + x) + x + \frac{5}{2}x^2 + \frac{11}{6}x^3 + \frac{1}{4}x^4 \right], \quad (\text{A25})$$

where $x \equiv \epsilon - 1$. Eq. (A25) was previously obtained by [Fabian et al. \(2001\)](#).

B. ORIENTATION-AVERAGED CROSS SECTIONS FOR PARTIALLY-ALIGNED GRAINS

Consider radiation propagating along the $\hat{\mathbf{z}}$ axis. Let the local magnetic field be in the $\hat{\mathbf{y}} - \hat{\mathbf{z}}$ plane, with $\gamma =$ the angle between $\hat{\mathbf{B}}$ and the line-of-sight: $\hat{\mathbf{B}} = \hat{\mathbf{y}} \sin \gamma + \hat{\mathbf{z}} \cos \gamma$. Let $\hat{\mathbf{J}}$ be a unit vector in the direction of the grain's angular momentum, and β the angle between $\hat{\mathbf{J}}$ and $\hat{\mathbf{B}}$. If $\beta > 0$, the grain's magnetic moment will cause $\hat{\mathbf{J}}$ to precess around $\hat{\mathbf{B}}$, and we may write

$$\hat{\mathbf{J}} = \hat{\mathbf{B}} \cos \beta + \hat{\mathbf{x}} \sin \beta \cos \phi_1 + (\hat{\mathbf{x}} \times \hat{\mathbf{B}}) \sin \beta \sin \phi_1 \quad (\text{B26})$$

$$= \hat{\mathbf{x}} \sin \beta \cos \phi_1 + \hat{\mathbf{y}} (\cos \beta \sin \gamma - \sin \beta \cos \gamma \sin \phi_1) + \hat{\mathbf{z}} (\cos \beta \cos \gamma + \sin \beta \sin \gamma \sin \phi_1), \quad (\text{B27})$$

with ϕ_1 varying from 0 to 2π over one precession period. Observations of starlight polarization indicate that there is systematic alignment of \mathbf{J} with \mathbf{B} , i.e., $\langle \cos^2 \beta \rangle > 1/3$, with the alignment presumed to result from some combination of paramagnetic dissipation (Davis & Greenstein 1951), superparamagnetic dissipation (Jones & Spitzer 1967), ferromagnetic dissipation (Draine & Hensley 2013) or starlight torques (Draine & Weingartner 1997; Weingartner & Draine 2003; Hoang & Lazarian 2009a,b).

On short time scales the grain spins and nutates with fixed $\hat{\mathbf{J}}$ according to the dynamics of rigid bodies (see, e.g., Weingartner & Draine 2003). Let $\hat{\mathbf{a}}_1$ be the principal axis of largest moment of inertia, and let α be the angle between $\hat{\mathbf{J}}$ and $\hat{\mathbf{a}}_1$. At constant J and kinetic energy E_{rot} the grain will tumble: $\hat{\mathbf{a}}$ will nutate around $\hat{\mathbf{J}}$. If the grain is triaxial, the angle α does not remain constant during the nutation, but will have some time-averaged value of $\langle \cos^2 \alpha \rangle$.

For fixed J , the kinetic energy of the grain is minimized if $\alpha = 0$ ($\cos^2 \alpha = 1$). If the direction of $\hat{\mathbf{a}}$ is uncorrelated with $\hat{\mathbf{J}}$, then $\langle \cos^2 \alpha \rangle = 1/3$. Thus we expect dissipation in the grain to result in $\langle \cos^2 \alpha \rangle > 1/3$. Suprathermally rotating grains, with rotational kinetic energy $E_{\text{rot}} \gg kT_{\text{grain}}$, are expected to have $\cos^2 \alpha \approx 1$ as the result of dissipation associated with viscoelasticity (Purcell 1979) or the even greater dissipation associated with the Barnett effect (Lazarian & Roberge 1997) and nuclear spin relaxation (Lazarian & Draine 1999).

After averaging over precession and nutation,

$$\langle (\hat{\mathbf{a}}_1 \cdot \hat{\mathbf{x}})^2 \rangle = \frac{1}{3} - \frac{3}{4} \left(\langle \cos^2 \alpha \rangle - \frac{1}{3} \right) \left(\cos^2 \beta - \frac{1}{3} \right) \quad (\text{B28})$$

$$\langle (\hat{\mathbf{a}}_1 \cdot \hat{\mathbf{y}})^2 \rangle = \frac{1}{3} + \frac{9}{4} \left(\langle \cos^2 \alpha \rangle - \frac{1}{3} \right) \left(\cos^2 \beta - \frac{1}{3} \right) \left(\sin^2 \gamma - \frac{1}{3} \right) \quad (\text{B29})$$

$$\langle (\hat{\mathbf{a}}_2 \cdot \hat{\mathbf{x}})^2 \rangle = \langle (\hat{\mathbf{a}}_3 \cdot \hat{\mathbf{x}})^2 \rangle = \frac{1}{3} + \frac{3}{8} \left(\langle \cos^2 \alpha \rangle - \frac{1}{3} \right) \left(\langle \cos^2 \beta \rangle - \frac{1}{3} \right) \quad (\text{B30})$$

$$\langle (\hat{\mathbf{a}}_2 \cdot \hat{\mathbf{y}})^2 \rangle = \langle (\hat{\mathbf{a}}_3 \cdot \hat{\mathbf{y}})^2 \rangle = \frac{1}{3} - \frac{9}{8} \left(\langle \cos^2 \alpha \rangle - \frac{1}{3} \right) \left(\cos^2 \beta - \frac{1}{3} \right) \left(\sin^2 \gamma - \frac{1}{3} \right) \quad (\text{B31})$$

The cross sections for radiation polarized in the $\hat{\mathbf{x}}$ and $\hat{\mathbf{y}}$ directions are

$$C_x = C_{\text{ran}} + \frac{2}{3}C_{\text{pol}}\Phi \quad (\text{B32})$$

$$C_y = C_{\text{ran}} - 2C_{\text{pol}}\Phi \left(\sin^2 \gamma - \frac{1}{3} \right) \quad (\text{B33})$$

$$\frac{C_x + C_y}{2} = C_{\text{ran}} - C_{\text{pol}}\Phi \left(\sin^2 \gamma - \frac{2}{3} \right) \quad (\text{B34})$$

$$\frac{C_x - C_y}{2} = C_{\text{pol}}\Phi \sin^2 \gamma \quad (\text{B35})$$

$$C_{\text{ran}} \equiv \frac{1}{3} [C_{\text{abs}}(\mathbf{E} \parallel \hat{\mathbf{a}}_1) + C_{\text{abs}}(\mathbf{E} \parallel \hat{\mathbf{a}}_2) + C_{\text{abs}}(\mathbf{E} \parallel \hat{\mathbf{a}}_3)] \quad (\text{B36})$$

$$C_{\text{pol}} \equiv \frac{1}{4} [C_{\text{abs}}(\mathbf{E} \parallel \hat{\mathbf{a}}_2) + C_{\text{abs}}(\mathbf{E} \parallel \hat{\mathbf{a}}_3) - 2C_{\text{abs}}(\mathbf{E} \parallel \hat{\mathbf{a}}_1)] \quad (\text{B37})$$

$$\Phi \equiv \frac{9}{4} \left(\langle \cos^2 \alpha \rangle - \frac{1}{3} \right) \left(\cos^2 \beta - \frac{1}{3} \right) . \quad (\text{B38})$$

C. ESTIMATING C_{ran} FROM OBSERVATIONS

Suppose that the attenuation I/I_0 is known, where the intensity $I(\lambda)$ is summed over both polarization modes, and the unattenuated radiation I_0 is unpolarized. The fractional polarization $p(\lambda)$ is also measured. Let $\hat{\mathbf{z}}$ be the direction of propagation, and $\hat{\mathbf{y}}$ be the polarization direction. If N is the total column density of grains, we seek to determine the cross section $C_{\text{ran}}(\lambda)$ for randomly-oriented grains. Define

$$\bar{\tau} \equiv \frac{\tau_x + \tau_y}{2} \quad (\text{C39})$$

$$\tau_p \equiv \frac{\tau_x - \tau_y}{2} . \quad (\text{C40})$$

Then

$$\frac{I}{I_0} = \frac{e^{-\tau_x} + e^{-\tau_y}}{2} \quad (\text{C41})$$

$$= e^{-\bar{\tau}} \left[1 - \frac{1}{2}\tau_p^2 + O(\tau_p^4) \right] . \quad (\text{C42})$$

$$p = \frac{e^{-\tau_y} - e^{-\tau_x}}{2I/I_0} \quad (\text{C43})$$

$$= \tau_p \frac{[1 + \frac{1}{6}\tau_p^2 + O(\tau_p^4)]}{[1 - \frac{1}{2}\tau_p^2 + O(\tau_p^4)]} = \tau_p \left[1 + \frac{2}{3}\tau_p^2 + O(\tau_p^4) \right] , \quad (\text{C44})$$

$$\tau_p \approx p - \frac{2}{3}p^3 + O(p^5) , \quad (\text{C45})$$

$$\bar{\tau} = \ln(I_0/I) + \ln \left[1 - \frac{1}{2}\tau_p^2 + O(\tau_p^4) \right] \quad (\text{C46})$$

$$\approx \ln(I_0/I) - \frac{1}{2}\tau_p^2 + O(\tau_p^4) \quad (\text{C47})$$

$$\approx \ln(I_0/I) - \frac{1}{2}p^2 + O(p^4) . \quad (\text{C48})$$

From (B34–B37) we have

$$\bar{\tau} = N \left[C_{\text{ran}} - C_{\text{pol}} \Phi \left(\sin^2 \gamma - \frac{2}{3} \right) \right] \quad (\text{C49})$$

$$= NC_{\text{ran}} - \tau_p \left(1 - \frac{2}{3 \sin^2 \gamma} \right) . \quad (\text{C50})$$

Using (C45) and (C48) we obtain

$$C_{\text{ran}} = \frac{1}{N} \left[\ln \left(\frac{I_0}{I} \right) + p \left(1 - \frac{2}{3 \sin^2 \gamma} \right) - \frac{1}{2} p^2 - \frac{2}{3} p^3 \left(1 - \frac{2}{3 \sin^2 \gamma} \right) + O(p^4) \right] . \quad (\text{C51})$$

If the polarization fraction $p \ll 1$, we may approximate $C_{\text{ran}} \approx (1/N) \ln(I_0/I)$. For finite $p \lesssim 0.2$, we can correct for the alignment if p is measured and $\sin^2 \gamma$ can be estimated.

D. PROOF OF UNIQUENESS

For an ellipsoid with semi-major axes $a_1 \leq a_2 \leq a_3$, the corresponding shape factors $L_1 \geq L_2 \geq L_3$ are given by Eq. (2,3). While we do not offer a proof that there is an $(a_2/a_1, a_3/a_1)$ corresponding to every possible (L_1, L_2, L_3) , we have implemented a numerical procedure that always returns a solution. In this note, we demonstrate that this solution is unique.

Suppose that $(a_2/a_1, a_3/a_1)$ corresponds to the desired (L_1, L_2, L_3) . Without loss of generality, let $a_1 = 1$. We may then rewrite

$$L_j = \frac{a_2 a_3}{2} \int_0^\infty \frac{dx}{(a_j^2 + x) [(1+x)(a_2^2 + x)(a_3^2 + x)]^{1/2}} . \quad (\text{D52})$$

Computing the derivatives

$$\frac{\partial L_1}{\partial a_2} = \frac{1}{2} \int_0^\infty \frac{a_3 x dx}{(1+x)^{3/2} (a_2^2 + x)^{3/2} (a_3^2 + x)^{1/2}} \quad (\text{D53})$$

$$\frac{\partial L_1}{\partial a_3} = \frac{1}{2} \int_0^\infty \frac{a_2 x dx}{(1+x)^{3/2} (a_2^2 + x)^{1/2} (a_3^2 + x)^{3/2}} \quad (\text{D54})$$

$$\frac{\partial L_2}{\partial a_3} = \frac{1}{2} \int_0^\infty \frac{a_2 x dx}{(1+x)^{1/2} (a_2^2 + x)^{3/2} (a_3^2 + x)^{3/2}} \quad (\text{D55})$$

$$\frac{\partial L_3}{\partial a_2} = \frac{1}{2} \int_0^\infty \frac{a_3 x dx}{(1+x)^{1/2} (a_2^2 + x)^{3/2} (a_3^2 + x)^{3/2}} , \quad (\text{D56})$$

we see that the integrands are positive definite for all a_2, a_3 , and x . Therefore,

$$\frac{\partial L_1}{\partial a_2} > 0 , \quad \frac{\partial L_1}{\partial a_3} > 0 , \quad \frac{\partial L_2}{\partial a_3} > 0 , \quad \frac{\partial L_3}{\partial a_2} > 0 . \quad (\text{D57})$$

Because the L_j sum to one, it must be true that

$$\frac{\partial L_1}{\partial a_2} + \frac{\partial L_2}{\partial a_2} + \frac{\partial L_3}{\partial a_2} = 0 \quad (\text{D58})$$

$$\frac{\partial L_1}{\partial a_3} + \frac{\partial L_2}{\partial a_3} + \frac{\partial L_3}{\partial a_3} = 0 , \quad (\text{D59})$$

and so

$$\frac{\partial L_2}{\partial a_2} < 0 \quad , \quad \frac{\partial L_3}{\partial a_3} < 0 \quad . \quad (\text{D60})$$

Assume that there are two sets of axial ratios (a_2, a_3) and (a'_2, a'_3) which yield the same (L_1, L_2, L_3) . We will proceed by starting from (a_2, a_3) and adjusting the axial ratios one at a time to the values (a'_2, a'_3) . We will show that it is impossible to make a nonzero adjustment and return back to the original (L_1, L_2, L_3) . Note that since $1 \leq a_2 \leq a_3$ by construction, $L_1 \geq L_2 \geq L_3$ and thus permutations of the L_j are excluded.

If $a_2 > a'_2$, we can first decrease a_2 until it is equal to a'_2 . From the realtions above, doing so decreases L_1 , increases L_2 , and decreases L_3 . To return the L_j to their original values, adjusting a_3 must increase L_1 , decrease L_2 , and increase L_3 . However, decreasing a_3 decreases L_1 while increasing a_3 increases L_2 , and so the desired adjustment is not possible. An analogous argument holds for $a_2 < a'_2$.

Therefore, (a_2, a_3) is the *unique* set of axial ratios corresponding to (L_1, L_2, L_3) .

REFERENCES

- Alexander, D. B., & Ferguson, J. W. 1994, in Lecture Notes in Physics, Berlin Springer Verlag, Vol. 428, IAU Colloq. 146: Molecules in the Stellar Environment, ed. U. G. Jorgensen, 149
- Altobelli, N., Postberg, F., Fiege, K., et al. 2016, *Science*, 352, 312, doi: [10.1126/science.aac6397](https://doi.org/10.1126/science.aac6397)
- Bohren, C. F., & Huffman, D. R. 1983, *Absorption and Scattering of Light by Small Particles* (New York: Wiley)
- Davis, L. J., & Greenstein, J. L. 1951, *ApJ*, 114, 206
- Draine, B. T., & Hensley, B. 2013, *ApJ*, 765, 159, doi: [10.1088/0004-637X/765/2/159](https://doi.org/10.1088/0004-637X/765/2/159)
- Draine, B. T., & Hensley, B. S. 2021, *ApJ*, accepted; arXiv:2009.11314
- Draine, B. T., & Lee, H. M. 1984, *ApJ*, 285, 89
- Draine, B. T., & Weingartner, J. C. 1996, *ApJ*, 470, 551, doi: [10.1086/177887](https://doi.org/10.1086/177887)
- . 1997, *ApJ*, 480, 633, doi: [10.1086/304008](https://doi.org/10.1086/304008)
- Fabian, D., Henning, T., Jäger, C., et al. 2001, *A&A*, 378, 228, doi: [10.1051/0004-6361:20011196](https://doi.org/10.1051/0004-6361:20011196)
- Gold, T. 1952, *MNRAS*, 112, 215
- Greenberg, J. M. 1968, *Interstellar Grains*, ed. B. M. Middlehurst & L. H. Aller (the University of Chicago Press), 221
- Hensley, B. S., & Draine, B. T. 2021, *ApJ*, 906, 73, doi: [10.3847/1538-4357/abc8f1](https://doi.org/10.3847/1538-4357/abc8f1)
- Hensley, B. S., Zhang, C., & Bock, J. J. 2019, *ApJ*, 887, 159, doi: [10.3847/1538-4357/ab5183](https://doi.org/10.3847/1538-4357/ab5183)
- Hoang, T. 2019, *ApJ*, 876, 13, doi: [10.3847/1538-4357/ab1075](https://doi.org/10.3847/1538-4357/ab1075)
- Hoang, T., & Lazarian, A. 2008, *MNRAS*, 388, 117, doi: [10.1111/j.1365-2966.2008.13249.x](https://doi.org/10.1111/j.1365-2966.2008.13249.x)
- . 2009a, *ApJ*, 695, 1457, doi: [10.1088/0004-637X/695/2/1457](https://doi.org/10.1088/0004-637X/695/2/1457)
- . 2009b, *ApJ*, 697, 1316, doi: [10.1088/0004-637X/697/2/1316](https://doi.org/10.1088/0004-637X/697/2/1316)
- Jones, R. V., & Spitzer, L. J. 1967, *ApJ*, 147, 943
- Kataoka, A., Muto, T., Momose, M., et al. 2015, *ApJ*, 809, 78, doi: [10.1088/0004-637X/809/1/78](https://doi.org/10.1088/0004-637X/809/1/78)
- Landau, L. D., Lifshitz, E. M., & Pitaevskii, L. P. 1993, *Electrodynamics of Continuous Media* (Oxford: Pergamon Press)
- Lazarian, A., & Draine, B. T. 1999, *ApJL*, 520, L67
- Lazarian, A., & Hoang, T. 2007, *MNRAS*, 378, 910, doi: [10.1111/j.1365-2966.2007.11817.x](https://doi.org/10.1111/j.1365-2966.2007.11817.x)
- Lazarian, A., & Roberge, W. G. 1997, *ApJ*, 484, 230, doi: [10.1086/304309](https://doi.org/10.1086/304309)
- Lee, H. M., & Draine, B. T. 1985, *ApJ*, 290, 211, doi: [10.1086/162974](https://doi.org/10.1086/162974)
- Martin, P. G. 1972, *MNRAS*, 159, 179
- . 1974, *ApJ*, 187, 461, doi: [10.1086/152655](https://doi.org/10.1086/152655)
- Min, M., Hovenier, J. W., & de Koter, A. 2003, *A&A*, 404, 35, doi: [10.1051/0004-6361:20030456](https://doi.org/10.1051/0004-6361:20030456)
- Min, M., Hovenier, J. W., Dominik, C., de Koter, A., & Yurkin, M. A. 2006, *JQSRT*, 97, 161, doi: [10.1016/j.jqsrt.2005.05.059](https://doi.org/10.1016/j.jqsrt.2005.05.059)
- Min, M., Hovenier, J. W., Waters, L. B. F. M., & de Koter, A. 2008, *A&A*, 489, 135, doi: [10.1051/0004-6361:200809534](https://doi.org/10.1051/0004-6361:200809534)
- Ossenkopf, V., Henning, T., & Mathis, J. S. 1992, *A&A*, 261, 567
- Press, W. H., Teukolsky, S. A., Vetterling, W. T., & Flannery, B. P. 1992, *Numerical recipes in FORTRAN. The art of scientific computing* (Cambridge: University Press, 2nd ed.)
- Purcell, E. M. 1979, *ApJ*, 231, 404
- Purcell, E. M., & Spitzer, Jr., L. 1971, *ApJ*, 167, 31, doi: [10.1086/151002](https://doi.org/10.1086/151002)

- Rho, J., Gomez, H. L., Boogert, A., et al. 2018, MNRAS, 479, 5101, doi: [10.1093/mnras/sty1713](https://doi.org/10.1093/mnras/sty1713)
- Rouleau, F., & Martin, P. G. 1991, ApJ, 377, 526, doi: [10.1086/170382](https://doi.org/10.1086/170382)
- Sargent, B., Forrest, W. J., D’Alessio, P., et al. 2006, ApJ, 645, 395, doi: [10.1086/504283](https://doi.org/10.1086/504283)
- Silsbee, K., & Draine, B. T. 2016, ApJ, 818, 133, doi: [10.3847/0004-637X/818/2/133](https://doi.org/10.3847/0004-637X/818/2/133)
- Tatsuuma, M., & Kataoka, A. 2021, arXiv e-prints, arXiv:2101.04910. <https://arxiv.org/abs/2101.04910>
- Tazaki, R., Lazarian, A., & Nomura, H. 2017, ApJ, 839, 56, doi: [10.3847/1538-4357/839/1/56](https://doi.org/10.3847/1538-4357/839/1/56)
- Treffers, R., & Cohen, M. 1974, ApJ, 188, 545
- van de Hulst, H. C. 1957, Light Scattering by Small Particles (New York: John Wiley & Sons)
- Weingartner, J. C., & Draine, B. T. 2003, ApJ, 589, 289, doi: [10.1086/374597](https://doi.org/10.1086/374597)
- Westphal, A. J., Bechtel, H. A., Brenker, F. E., et al. 2014a, Meteor. Plan. Sci., 49, 1720, doi: [10.1111/maps.12221](https://doi.org/10.1111/maps.12221)
- . 2014b, Science, 345, 786
- Zubko, V. G., Mennella, V., Colangeli, L., & Bussoletti, E. 1996, MNRAS, 282, 1321